Journal of *Marine Science and Engineering*

MDPI

Article

Optimal Design and Performance Analysis of a Hybrid System Combining a Semi-Submersible Wind Platform and Point Absorbers

Binzhen Zhou [1], Jianjian Hu [1], Qi Zhang [1], Lei Wang [1,*], Fengmei Jing [2] and Maurizio Collu [3]

[1] School of Civil Engineering and Transportation, South China University of Technology, Guangzhou 510641, China; zhoubinzhen@scut.edu.cn (B.Z.); hjj1834619@163.com (J.H.); 202210181578@mail.scut.edu.cn (Q.Z.)
[2] School of Mechanical Engineering, Beijing Institute of Petrochemical Technology, Beijing 102617, China; jingfengmei@bipt.edu.cn
[3] Naval Architecture, Marine and Ocean Engineering Department, University of Strathclyde, Glasgow G4 0LZ, UK; maurizio.collu@strath.ac.uk
* Correspondence: wangleimme@scut.edu.cn

Abstract: Integrating point absorber wave energy converters (PAWECs) and an offshore floating wind platform provide a cost-effective way of joint wind and wave energy exploitation. However, the coupled dynamics of the complicated hybrid system and its influence on power performance are not well understood. Here, a frequency-domain-coupled hydrodynamics, considering the constraints and the power output through the relative motion between the PAWECs and the semi-submersible platform, is introduced to optimize the size, power take-off damping, and layout of the PAWECs. Results show that the annual wave power generation of a PAWEC can be improved by 30% using a 90° conical or a hemispherical bottom instead of a flat bottom. Additionally, while letting the PAWECs protrude out the sides of the triangular frame of the platform by a distance of 1.5 times the PAWEC radius, the total power generation can be improved by up to 18.2% without increasing the motion response of the platform. The PAWECs can reduce the resonant heave motion of the platform due to the power take-off damping force. This study provides a reference for the synergistic use of wave and wind energy.

Keywords: absorber wave energy converter; floating wind platform; hybrid system; wave power; hydrodynamic performance

Citation: Zhou, B.; Hu, J.; Zhang, Q.; Wang, L.; Jing, F.; Collu, M. Optimal Design and Performance Analysis of a Hybrid System Combining a Semi-Submersible Wind Platform and Point Absorbers. *J. Mar. Sci. Eng.* **2023**, *11*, 1190. https://doi.org/10.3390/jmse11061190

Academic Editors: Eugen Rusu, Kostas Belibassakis and George Lavidas

Received: 10 May 2023
Revised: 29 May 2023
Accepted: 6 June 2023
Published: 8 June 2023

1. Introduction

Wave energy, characterized by high energy density and predictability, is regarded as one of the potential renewable energy sources [1]. More than a thousand novel wave energy converters (WECs) have been designed [2], which can be roughly categorized into the oscillating water column (OWC) [3–5], the oscillating body [6,7], and the overtopping. However, the high cost of the operation and maintenance of WECs impedes their commercial use. Researchers have actively sought solutions to reduce the cost and improve the power performance of WECs. A plausible way is to combine the WECs with existing marine structures [8–10].

Combining WECs with a floating offshore wind platform to form a hybrid system brings several benefits. The seas with abundant wind resources are also rich in wave energy resources [11], providing a feasible premise for hybridization. The wind platform could provide an installation base and share moorings, grids, and maintenance with the WECs, which reduces the cost of the WECs. In return, the WECs may form a protective shield between the incident waves and wind turbines, reducing direct wave impact on the support structures and creating a more stable operating environment for the wind turbines [12–15].

The generated wave power could also compensate for the power output shortage due to downtime [16].

Till now, most of the wind–wave hybrid system concepts have resulted from the renowned EU FP7 MARINA platform project [17]. The power and dynamic performance of these hybrid systems were primarily explored. M'zoughi et al. [18] studied a hybrid system consisting of two OWCs and an NREL 5MW wind turbine. They showed that OWCs reduced the pitch motion of the platform and the fore-aft displacement of the tower top, improving the stability of the platform. Further, Aboutalebi et al. [19] proposed a novel barge platform with four OWCs, which oscillated less than the original barge platform in the prescribed range of waves. Compared with OWCs, the oscillating body WECs are easier to be integrated onto a wind platform without retrofitting too much of the platform. The representative hybrid systems consisting of oscillating body WECs are SFC (Semi-submersible Flap Combination) [20,21] and STC (Spar Torus Combination) [22]. Michailides et al. [20] found that the flap WECs did not affect the mooring tension, the nacelle acceleration, or the bending moment in the tower base of SFC. Subsequent experiments on SFC under extreme wave conditions showed no strong nonlinear hydrodynamic phenomenon was observed [21]. Other hybrid systems, including flap WECs, are the WaveStar series [23]. However, Karimirad and Michailides [24] showed that the flap WECs could increase the overall wave excitation moment hence the pitch motion of the wind turbine. On the other hand, the hybrid systems consisting of heaving oscillating body WECs do not suffer from this instability increase, therefore, are a more preferred hybridization form.

The hybrid systems consisting of heaving WECs and a floating wind platform have been extensively studied numerically, most of which are in the time domain. Muliawan et al. [22] used a combined time-domain toolkit SIMO/ TDHMILL3D to analyze the coupled dynamics of STC under joint wind and wave loads. The generated wind and wave energy were pointed out to be synergized well under given operational conditions. Cheng et al. [25] studied the hybrid system of a spar-type VAWT (vertical-axis wind turbine) and an annular WEC using a time-domain SIMO-RIFLEX-DMS toolkit based on potential flow theory and Morrison equation. Compared with a single VAWT, the WEC promoted the power output and reduced the mooring tension and low-frequency responses in heave and pitch. Ren et al. [26] studied the TWWC (TLP-WT-WEC-Combination) hybrid system through a time-domain scheme modeled in ANSYS/AQWA module. Wang et al. [27] combined an OC4 semi-submersible platform with an annular heaving WEC on the central column of the platform. The investigation was also carried out in the time domain using ANSYS/AQWA. The constraint between the WEC and the platform was modeled as a fender, which is time-consuming in computation. They found that the WEC with a concave bottom generated more power and moved mildly [28].

Compared with the time-domain models, the frequency-domain models are more effective in works such as optimizing layouts of WECs in the hybrid system. Hu et al. [29] proposed a frequency-domain model with a fixed platform to vigorously investigate the influence of the diameter-to-draft ratio and layouts of several WECs on the power performance and external loads on the hybrid system consisting of a WindFloat platform and heaving cylindrical point absorber WECs. They developed a fast optimization method to determine the size and layouts of the WECs according to the operational condition. Further, Zhou et al. [30] expanded the investigation on the influence of WEC bottom shapes and found that a hemispherical bottom brings the most power generation, better than a conical bottom and much better than a flat bottom. Later, Zhou et al. [31] established a more complete frequency-domain model supplemented by the previous, considering constrained dynamics and multiple DoF motion responses.

Although the frequency-domain model in Hu et al. [29] and Zhou et al. [30] was quick in optimizing the WECs and wave loads analysis, the platform is fixed for simplicity. Only the heave motion of the WECs is considered, whereas the coupled dynamics and the effect of mooring in the hybrid system are not included. In real situations, there are constraints between the WECs and the platforms, and the hybrid system can move

in multiple degrees of freedom (DoFs), which are important in determining the power generation and dynamic features of the hybrid system. In this paper, these important effects are studied through a hybrid system consisting of an OC4 wind platform and several heaving point absorber WECs using this frequency-domain coupled hydrodynamic model proposed by Zhou et al. [31]. The novelties are: first, the influence of bottom shape and size of the WECs on the power performance and dynamic response of the hybrid system are explored; second, the WECs are further deployed protruding the triangular frame of the wind platform. The influence of the protruding length on the performance of the system is investigated, which are rarely seen in previous studies. An optimal layout of the WECs is yielded.

The rest of the paper is structured as follows. Section 2 describes the configuration of the platform and WECs. Section 3 introduces the constrained coupled multi-body model based on potential flow theory with viscous correction in the frequency domain. Section 4 investigates the influence of WEC bottom shapes and layout on both wave power performance and motion response of the hybrid system. Finally, conclusions are presented in Section 5.

2. Configuration of the Hybrid System

2.1. Floating Wind Platform and WECs

A hybrid system consisting of a floating wind platform and multiple heaving wave energy converters is illustrated in Figure 1. The widely applied OC4-DeepCwind semi-submersible platform [32], installed with a 5 MW wind turbine above the central column, is selected as a representative of the present hybrid system. Its key parameters are shown in Table 1. Heaving WECs with power take-off (PTO) systems are arranged on the sides of the platform between the pontoons. The platform allows six-degree-of-freedom motions for various incident waves, whereas the WECs, constrained by PTO systems, can only slide along the vertical poles on the pontoons, consequently generating electricity through the relative heave motion against the platform.

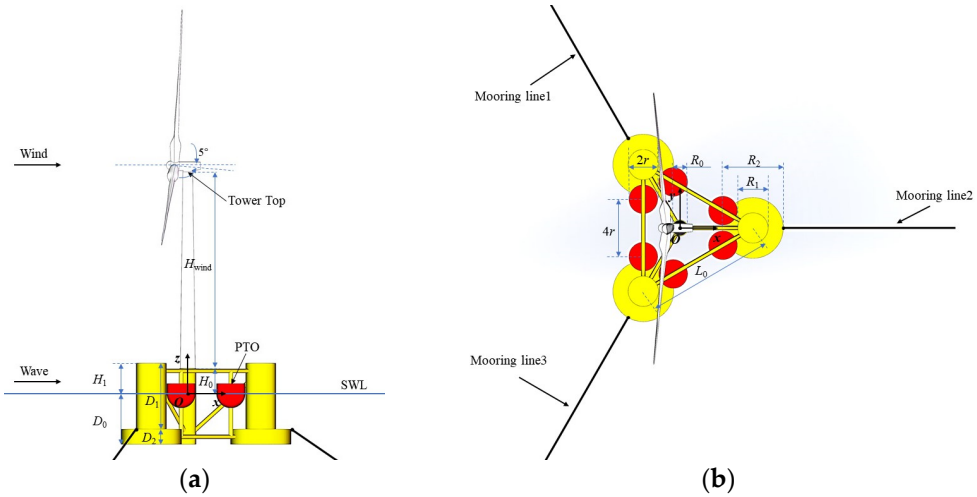

Figure 1. Diagram of the hybrid system consisting of an OC4-DeepCwind semi-submersible platform and multiple heaving WECs: (**a**) Side view; (**b**) Top view.

Table 1. Main dimensions of OC4-DeepCwind semi-submersible platform.

Parameter	Symbol	
Diameter of main column	R_0	6.5 m
Diameter of offset (upper) columns	R_1	12 m
Diameter of base columns	R_2	24 m
Diameter of pontoons and cross braces	R_3	1.6 m

Table 1. *Cont.*

Parameter	Symbol	
Spacing between offset columns	L_0	50 m
Total draft	D_0	20 m
Height of upper columns	D_1	26 m
Height of base columns	D_2	6 m
Elevation of main column above SWL	H_0	10 m
Elevation of offset columns above SWL	H_1	12 m
Height of tower	H_{wind}	77.6m
Total platform mass	M_0	1.3473×10^7 kg
Position of mass center below water surface	CM_0	13.46 m
Total roll moment of inertia (about mass center)	$I_{22} + I_{33}$	6.827×10^9 kg·m^2
Total pitch moment of inertia (about mass center)	$I_{11} + I_{33}$	6.827×10^9 kg·m^2
Total yaw moment of inertia (about mass center)	$I_{11} + I_{22}$	$1.2236E \times 10^{10}$ kg·m^2
Resonance period in surge direction	T_{surge}	104.7 s
Resonance period in heave direction	T_{heave}	17.5 s
Resonance period in pitch direction	T_{pitch}	20.6 s

2.2. Mooring System

A three-catenary mooring system is assorted to the platform (Figure 2). The property and arrangement of the mooring lines can be referred to in Ref. [32]. The mooring system is converted to an equivalent stiffness matrix (Table 2) by the open-source code Mooring Analysis Program (MAP) [33] for the coming frequency-domain analysis.

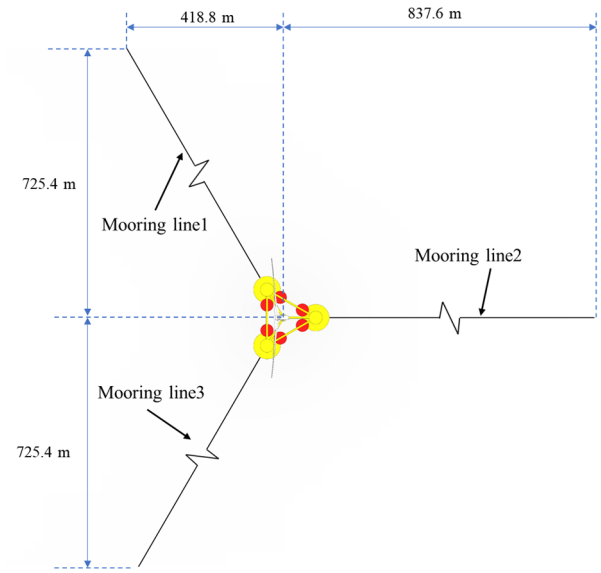

Figure 2. Diagram of mooring arrangement.

Table 2. Equivalent mooring stiffness matrix.

	Surge	Sway	Heave	Unit	Roll	Pitch	Yaw	Unit
Surge	6.08×10^4	-2.51×10^{-2}	-2.84×10^{-2}	kg·s^{-2}	4.72×10^1	-1.05×10^5	6.25×10^{-1}	kg·m·s^{-2}·rad^{-1}
Sway	2.40×10^{-1}	6.08×10^4	-1.21×10^{-2}	kg·s^{-2}	1.05×10^5	4.66×10^1	1.46×10^0	kg·m·s^{-2}·rad^{-1}
Heave	-2.40×10^{-2}	2.61×10^{-1}	1.83×10^4	kg·s^{-2}	2.76×10^{-1}	1.44×10^{-1}	9.40×10^1	kg·m·s^{-2}·rad^{-1}
Roll	4.71×10^1	1.06×10^5	-2.63×10^{-2}	kg·m·s^{-2}	8.38×10^7	3.00×10^3	1.96×10^1	kg·m^2·s^{-2}·rad^{-1}
Pitch	-1.06×10^5	4.70×10^1	1.04×10^{-1}	kg·m·s^{-2}	-2.93×10^{-3}	8.38×10^7	1.27×10^1	kg·m^2·s^{-2}·rad^{-1}
Yaw	5.19×10^{-1}	1.47×10^0	-9.38×10^1	kg·m·s^{-2}	2.58×10^1	1.55×10^1	1.12×10^8	kg·m^2·s^{-2}·rad^{-1}

2.3. Wave Environments

The WECs are designed, and the power performance of the hybrid system is evaluated according to field wave data measured at the Shidao site in Shandong Province, China. The joint probability distribution S_{ij} of wave height H_i and wave period T_j is given in Table 3. The average wave period T = 5.18 s is chosen for the WECs design to capture the maximum power.

Table 3. Joint distribution of wave height and wave period at Shidao in Shandong Province, China (unit: %).

S_{ij} T_j(s) / H_i(m)	3.0	4.0	5.0	6.0	7.0	8.0	9.0	10.0	11.0	12.0	13.0	14.0	Sum
0.2	0.0	0.0	0.0	0.0	0.0	0.0	0.0	0.0	0.0	0.0	0.0	0.0	0.1
0.3	0.1	2.4	3.2	1.5	0.3	0.1	0.0	0.0	0.0	0.0	0.0	0.0	7.6
0.4	0.2	10.3	15.8	5.4	1.5	0.4	0.1	0.0	0.0	0.0	0.0	0.0	33.8
0.5	0.0	3.6	7.5	5.3	2.2	0.9	0.5	0.2	0.1	0.0	0.0	0.0	20.3
0.6	0.0	1.8	3.8	3.3	2.1	0.4	0.4	0.1	0.1	0.0	0.0	0.0	12.1
0.7	0.0	0.6	2.6	2.2	0.9	0.1	0.2	0.1	0.1	0.0	0.0	0.0	7.0
0.8	0.0	0.2	2.2	1.4	0.9	0.1	0.0	0.0	0.1	0.0	0.0	0.0	5.0
0.9	0.0	0.1	1.1	1.0	0.8	0.2	0.1	0.1	0.0	0.0	0.0	0.0	3.5
1.0	0.0	0.1	0.6	0.9	0.7	0.2	0.1	0.0	0.1	0.0	0.0	0.0	2.6
1.1	0.0	0.0	0.2	0.6	0.6	0.1	0.0	0.0	0.0	0.0	0.1	0.1	1.7
1.2	0.0	0.0	0.1	0.5	0.5	0.1	0.0	0.0	0.0	0.0	0.1	0.0	1.4
1.3	0.0	0.0	0.0	0.4	0.4	0.1	0.0	0.0	0.0	0.0	0.0	0.0	1.0
1.4	0.0	0.0	0.0	0.3	0.3	0.2	0.0	0.0	0.0	0.0	0.0	0.0	1.0
1.5	0.0	0.0	0.0	0.2	0.4	0.0	0.1	0.0	0.1	0.0	0.0	0.0	0.8
1.6	0.0	0.0	0.0	0.1	0.1	0.1	0.1	0.0	0.0	0.0	0.0	0.0	0.6
1.7	0.0	0.0	0.0	0.1	0.2	0.2	0.1	0.1	0.0	0.0	0.0	0.0	0.6
1.8	0.0	0.0	0.0	0.1	0.1	0.0	0.0	0.0	0.0	0.0	0.0	0.0	0.3
1.9	0.0	0.0	0.0	0.0	0.1	0.1	0.1	0.0	0.0	0.0	0.0	0.0	0.3
2.0	0.0	0.0	0.0	0.0	0.0	0.0	0.1	0.0	0.0	0.0	0.0	0.0	0.2
2.1	0.0	0.0	0.0	0.0	0.0	0.0	0.0	0.0	0.0	0.0	0.0	0.0	0.1
Sum	0.3	19.1	37.3	23.3	12.0	3.4	2.1	1.0	0.9	0.3	0.3	0.2	100.0

3. Mathematical Model

3.1. Coupled Motion Equation of the Hybrid System

Frequency analysis is usually carried out with the following assumptions: the fluid is inviscid, incompressible, and irrotational, and the wave amplitude is small. The linear wave theory is applicable. The PTO systems and the mooring system are also modeled as linear. Hu et al. [29] developed a numerical model based on potential flow theory with viscous correction in the frequency domain, assuming the platform is fixed. However, when the floating platform moves, hydrodynamic interactions between the semi-submersible platform and WECs will be too sophisticated to be ignored, and the motion equation given by Hu et al. [29] cannot be suitable. Therefore, coupled motion equations considering complex interactions must be deduced to accurately describe the relative motion between multiple floating bodies.

The system, without considering the constraints, has $6(N + 1)$ motion modes, wherein the first $6N$ are assigned to the WECs, and the last six are to the platform. The motion equation for the i-th ($i = 1, \ldots, 6N$) mode of the WECs in incident wave with angular frequency ω is

$$\sum_{j=1}^{6(N+1)} \left[-\omega^2\left(m_{ij}+\mu_{ij}\right)-\mathrm{i}\omega\left(\lambda_{ij}+b_{\mathrm{vis},ij}\right)+C_{ij}+k_{\mathrm{stiff},ij}\right]x_j-\sum_{j=1}^{6(N+1)}\mathrm{i}\omega b_{\mathrm{PTO},ij}x_j=f_{\mathrm{ex},i}+\delta_{\mathrm{L},i}f_{\mathrm{L},i} \quad (1)$$

and the motion equation for the i-th ($i = 6N + 1, \ldots, 6(N + 1)$) mode of the platform is

$$\sum_{j=1}^{6(N+1)} \left[-\omega^2(m_{ij}+\mu_{ij}) - \mathrm{i}\omega(\lambda_{ij}+\lambda_{\mathrm{vis},ij}) + C_{ij} + k_{\mathrm{stiff},ij}\right] x_j - \sum_{j=1}^{6(N+1)} \mathrm{i}\omega b_{\mathrm{PTO},ij} x_j = f_{\mathrm{ex},i} - \sum_{n=0}^{N-1} \delta_{\mathrm{L},6n+i-6N} f_{\mathrm{L},6n+i-6N} \quad (2)$$

where m_{ij}, μ_{ij}, λ_{ij}, and C_{ij} are the elements of the mass, added mass, radiation damping, and hydrostatic restoration coefficient matrix in the ij-th mode, respectively. $b_{\mathrm{PTO},ij}$ is the ij-th term of the PTO damping matrix $\mathbf{B}_{\mathrm{PTO}}$. $k_{\mathrm{stiff},ij}$ is the ij-th term in the mooring stiffness matrix $\mathbf{K}_{\mathrm{stiff}}$, listed in Table 2. x_i, $f_{\mathrm{ex},i}$, and $f_{\mathrm{L},i}$ represent wave-excited motion response, wave excitation force, and constraint forces. $\Sigma\delta_{\mathrm{L},6n+i-6N} f_{\mathrm{L},6n+i-6N}$ is the total constraint force exerted by the WECs. For more details on the present implementation, readers can refer to Zhou et al. [31].

According to the continuous displacement condition at the connection between WECs and the platform, Sun et al. [34] introduced the constraint matrix $\mathbf{D}$ and obtained the following matrix equation.

$$\mathbf{L} = -\omega^2(\mathbf{m}+\boldsymbol{\mu}) - i\omega(\boldsymbol{\lambda}+\boldsymbol{\lambda}_{\mathrm{vis}}+\mathbf{B}_{\mathrm{PTO}}) + \mathbf{C} + \mathbf{K} \quad (3)$$

$$\begin{bmatrix} \mathbf{L}_{6(N+1)\times 6(N+1)} & \mathbf{D}^T_{6(N+1)\times 5N} \\ \mathbf{D}_{5N\times 6(N+1)} & 0 \end{bmatrix} \begin{bmatrix} \boldsymbol{\xi}_{6(N+1)} \\ \mathbf{f}_{\mathrm{L},5N} \end{bmatrix} = \begin{bmatrix} \mathbf{f}_{\mathrm{ex},6(N+1)} \\ 0 \end{bmatrix} \quad (4)$$

in which L is the coupling equation of the motion of the platform and WECs after removing the binding force. The constraint matrix $\mathbf{D}$ can be expressed as

$$\mathbf{D}_{5N\times 6(N+1)} = \begin{bmatrix} \varepsilon_1\mathbf{D}^1_1 & \cdots & 0 & \cdots & 0 & \varepsilon_{N+1}\mathbf{D}^1_{N+1} \\ \vdots & \ddots & \vdots & 0 & \vdots & \vdots \\ 0 & \cdots & \varepsilon_n\mathbf{D}^n_m & \cdots & 0 & \varepsilon_{N+1}\mathbf{D}^i_{N+1} \\ \vdots & 0 & \vdots & \ddots & \vdots & \vdots \\ 0 & \cdots & 0 & \cdots & \varepsilon_N\mathbf{D}^N_N & \varepsilon_{N+1}\mathbf{D}^N_{N+1} \end{bmatrix} \quad (5)$$

3.2. Power Generated by WECs

The wave power $P_n(T)$ generated by the n-th WEC is

$$P_n(T) = \frac{1}{2}\left(\frac{2\pi}{T}\right)^2 b^n_{\mathrm{PTO},3}|z_{\mathrm{rel},n}|^2 \quad (6)$$

where z_i is the relative heave displacement between the i-th WEC and the platform. The numerical scheme for searching for optimal PTO damping has been proposed by Hu et al. [29], with detailed explanations given in our previous work [31].

The total wave power $P_{\mathrm{total}}(T)$ of the WEC array and the annual wave power per unit weight $P_{\mathrm{total}}(\mathrm{year})$ are

$$P_{\mathrm{total}}(T) = \sum_{n=1}^{N} P_n(T) \quad (7)$$

$$P_{\mathrm{total}(year)}(T) = \sum_{j=1}^{M_j}\sum_{i=1}^{M_i}\left(\frac{H_i}{2}\right)^2 \times P_{\mathrm{total}}(T_j) \times S_{ij} \quad (8)$$

where P_n is the wave power of the n-th WEC under optimal PTO damping. M_i and M_j are the numbers of wave height and wave period listed in Table 3. H_i, T_j, and S_{ij} are the wave height, wave period, and the joint distribution introduced in Table 3.

3.3. Validation

Figure 3 compares the motion obtained from the above model with the published WEC-Sim results from Ruehl et al. [34]. The maximum difference in motion response is

beneath 3.0%. The overall agreement verifies the validity of the present model in simulating the multi-floating-body coupled constraint motion.

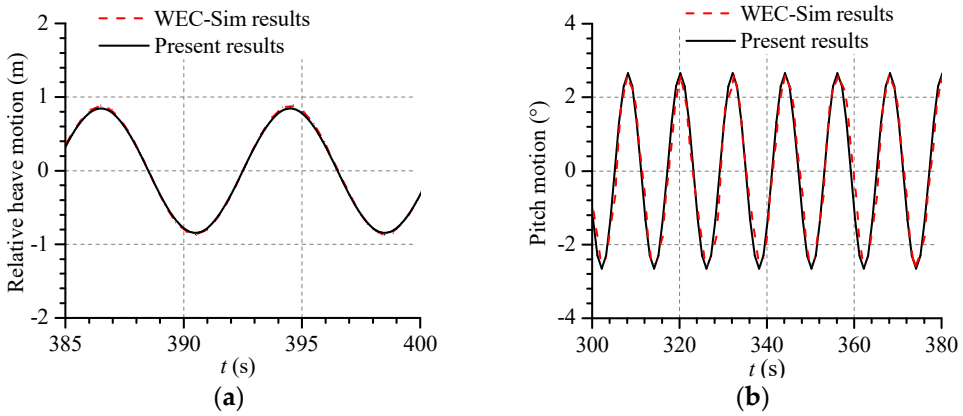

Figure 3. Comparison of the relative heave motion between WEC and spar and pitch motion between the present results and the published numerical results using WEC−Sim code: (**a**) Relative heave motion (b_{pto} = 1200.0 kN·s/m, T = 8.0 s); (**b**) Pitch motion (b_{pto} = 0.0 kN·s/m, T = 12.0 s).

4. Numerical Results and Discussion

In the numerical calculation of this hybrid system, the interaction of hydrodynamic forces, restraining forces, and PTO forces between the platform and the wave energy device are considered, while the influence of aerodynamic forces is ignored. The water depth h equals 200 m, and the wave height H is 2 m. The wave period range of the incident regular wave is taken as 3.0~20 s. The constrained motion satisfying the linear assumption ensures that, except for the heave direction, the motion of WECs in other directions is the same as that of the platform. Additionally, the linear PTO stiffness is set as 0, and the optimal PTO damping corresponds to the value when wave power generation reaches the maximum in the sea state with different wave periods.

4.1. Geometric Configurations of WECs

The geometric configuration of WECs will affect the synergistic performance of the hybrid system. Inspired by Zhou et al. [30], WECs with a flat bottom, conical bottom with conical angle α = 90°, and hemispherical bottom are explored. The dimensionless method [29] is an optimal choice to quickly determine the size of WECs, according to the typical or average wave frequency ω_p of the wave environment and the given value of diameter draft ratio $2r/d$ (r and d are the radius and draft of each WEC).

$$d = g\left(\frac{\overline{\omega}_n(2r/d)}{\omega_p}\right)^2 \tag{9}$$

Setting the working period at T = 5.18 s, the dimensions of WEC with cylindrical bottom corresponding to different diameter draft ratios ($2r/d$ = 3.0, 2.5, 1.5, 1.0) are obtained by the dimensionless method. Additionally, keeping the draft equivalent, dimensions of WECs with 90° conical bottom and hemispherical bottom corresponding to cylindrical WEC can be calculated, given in Table 4. The total damping, radiation damping, and viscosity correction coefficient $f_{\lambda,vist}$ can be obtained from the Star CCM+ free decay test [35,36].

Table 4. Parameters of WECs with different bottom shapes.

2r/d	Bottom Shape	d_1 * (m)	d_2 * (m)	2r (m)	n	Total Damping (kg·s^{-2})	Radiation Damping (kg·s^{-2})	$f_{\lambda,vist}$
3.0	flat	3.779	0.000	11.338	6	1.7639×10^5	9.1514×10^4	1.93
	90° conical	1.890	5.669	11.338		1.2728×10^5	1.2470×10^5	1.02
	hemispherical	0.000	5.669	11.338		1.2448×10^5	1.2939×10^5	0.98
2.5	flat	4.016	0.000	10.040	6	1.2577×10^5	5.9640×10^4	2.11
	90° conical	2.343	5.020	10.040		8.3451×10^4	7.7353×10^4	1.08
	hemispherical	0.669	5.020	10.040		7.9106×10^4	7.7482×10^4	1.02
1.5	flat	4.758	0.000	7.137	9	5.8053×10^4	1.2687×10^4	4.58
	90° conical	3.568	3.568	7.137		3.7767×10^4	1.9031×10^4	1.98
	hemispherical	2.379	3.568	7.137		2.8194×10^4	1.9446×10^4	1.45
1.0	flat	5.216	0.000	5.216	12	3.4508×10^4	4.6660×10^3	7.40
	90° concal	4.346	2.608	5.216		2.2355×10^4	5.7253×10^3	3.91
	hemispherical	3.477	2.608	5.216		2.0443×10^4	5.7923×10^3	3.53

* The submerged part of WECs under the still water level (SWL) with different bottom shapes is composed of one or two part(s): the vertical cylindrical part is denoted as d_1, and the non-flat bottom part d_2.

4.2. Layout Selection of WECs

WECs are arranged in the following way, the distance between float centers $L_1 = 4r$, the distance between float and center of the pontoon outside the platform $L_2 > r + R$, and the maximum number of WECs on one side of the truss round-up to $(L - 2(R + r))/4r$. Layouts of the flat bottom-shaped WEC with various $2r/d$ are given in Table 5. Corresponding arrangements combined with the OC4 platform are displayed in Figure 4.

Table 5. Layout of cylindrical WEC with flat bottom.

2r/d	d (m)	2r (m)	n	L_1 (m)	L_2 (m)
3.00	3.779	11.338	6	22.676	13.662
2.50	4.016	10.040	6	20.080	14.960
1.50	4.758	7.137	9	14.274	10.726
1.00	5.216	5.216	12	10.432	9.353

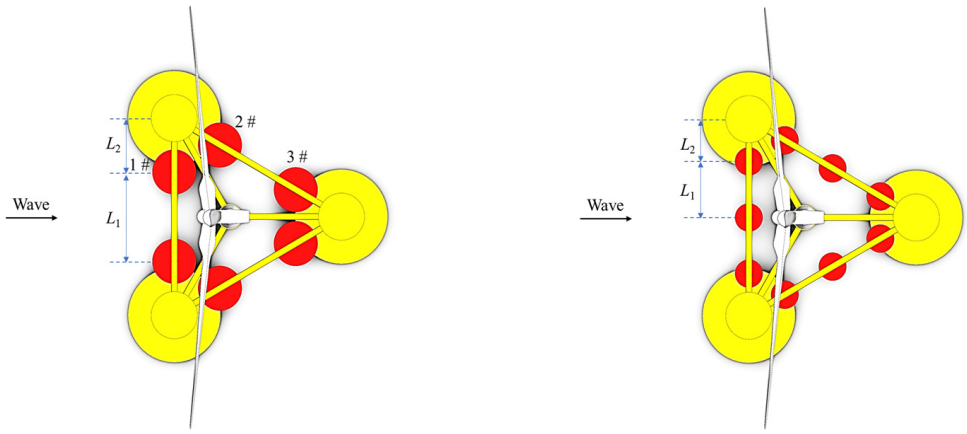

(a) (b)

Figure 4. *Cont.*

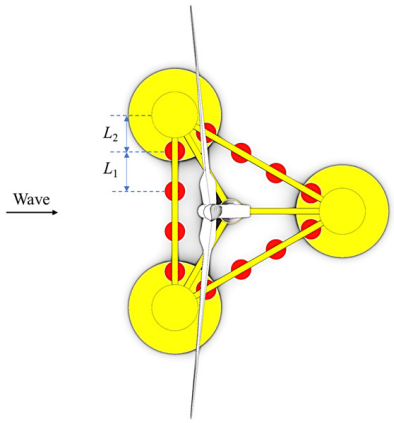

(**c**)

Figure 4. Arrangement of WEC combined with OC4 floating platform: (**a**) 6 WECs; (**b**) 9 WECs; (**c**) 12 WECs.

4.3. Wave Power of WECs

4.3.1. Wave Power with Different 2r/d

Power performance is the key index to test whether the hybrid system integrates well. Total wave power P_{total} versus incident wave periods for WECs with different bottom shapes are compared in Figure 5. For the same $2r/d$, the performance of wave power for WEC with the hemispherical bottom is almost as good (Figure 5a,b,d) or slightly better (Figure 5c) as that with the conical bottom. The total wave power of both these two is larger than that of WEC, with a flat bottom in all incident waves for various values of $2r/d$. Specifically, the annual wave power of WEC with a 90° conical bottom and with a hemispherical bottom increases by 32.5%/35.1%, 26.0%/29.1%, 27.2%/43.0%, and 24.7%/29.2% compared with cylindrical WEC with the flat bottom when $2r/d$ = 3.0, 2.5, 1.5, and 1.0, respectively. It is consistent with Zhou et al.'s discovery [29] that the single WEC with hemispherical bottom has the best energy conversion performance without being combined on the wind platform.

The variation of total wave power for various $2r/d$ is similar; that is, it gradually increases until the peak value, fluctuates near the peak, and then decreases gradually. Additionally, as the value of $2r/d$ becomes smaller, total wave power decreases. That means larger WECs are preferred in capturing more wave energy in a specific sea state, coincident with the hybrid system consisting of a WindFloat platform with a 5 MW wind turbine [29].

Additionally, the resonance period of WECs shifts down to a smaller period due to the coupling hydrodynamic forces between the platform and WECs; a phenomenon also observed in Hu et al.'s research [29]. Further, the offset amplitudes for WECs with a 90° conical bottom and a hemispherical bottom are larger than that with a flat bottom when the value of $2r/d$ is fixed. The resonance period for WEC with a 90° conical bottom and with hemispherical bottom was 4.65 s/4.62 s, 4.65 s/4.62 s, 4.91 s/4.91 s, and 4.99 s/4.99 s, while for WEC with a flat bottom is 4.83 s, 4.83 s, 5.11 s, and 5.15 s, corresponding to $2r/d$ = 3.0, 2.5, 1.5, and 1.0, respectively. Moreover, for WEC with the same bottom shape, the offset amplitude of the resonance period increases as $2r/d$ increases.

4.3.2. Relative Heave at Different Positions

For further explanation, optimal PTO damping and relative heave motion (its two main factors) versus incident wave periods at three different locations (1#, 2#, and 3#, illustrated in Figure 4a) of the hybrid system are explored in Figure 6, taking the case of $2r/d$ = 3.0 for example.

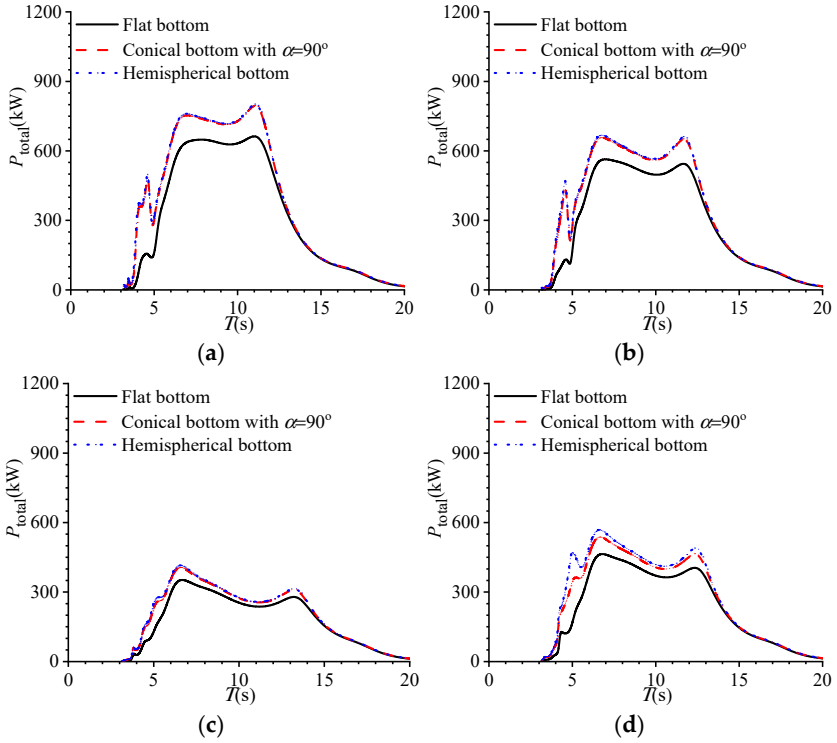

Figure 5. Comparisons of total wave power of the hybrid system with flat, 90° conical, and hemispherical bottoms for various values of $2r/d$: (**a**) $2r/d$ = 3.0; (**b**) $2r/d$ = 2.5; (**c**) $2r/d$ = 1.5; (**d**) $2r/d$ = 1.0.

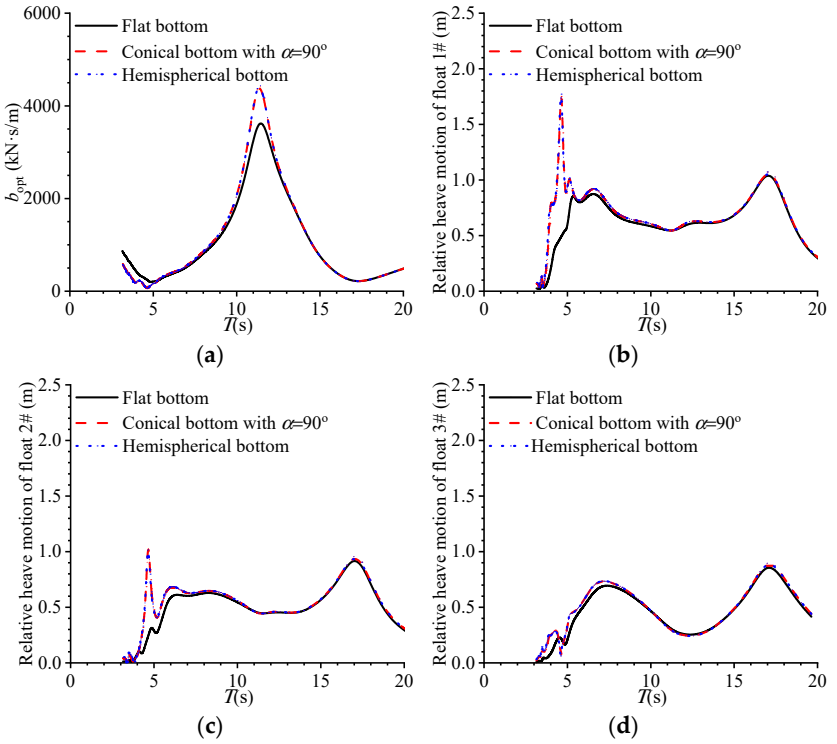

Figure 6. The optimal PTO damping and relative heave motion versus incident wave period of WECs with different bottom shapes in the case of $2r/d$ = 3.0: (**a**) b_{opt}; (**b**) Float 1#; (**c**) Float 2#; (**d**) Float 2#.

Near the resonance period (T = 5.18 s) of the target sea, optimal PTO damping of WECs with all three bottom shapes has little difference and is quite small. Compared to the cylindrical WEC with a flat bottom, the offset of the relative heave motion of WECs with

90° conical and hemispherical bottoms is quite large at location 1#, moderate at location 2#, and small at location 3#. These facts lead to the total wave power not reaching the peak near the resonance period, and the value corresponding to WECs with 90° conical and hemispherical bottoms is more significant than that with a flat bottom.

Near T = 12.0 s, optimal PTO damping reaches the peak, and the increased values of WECs with 90° conical and hemispherical bottoms are relatively large compared to a cylindrical WEC with a flat bottom. The relative heave motion of WECs with all three bottom shapes has little difference and is quite small at locations 1#, 2#, and 3#. This creates the phenomenon that the total wave power presents relatively upward near T = 12.0 s.

4.4. Platform Motion and Mooring Force

4.4.1. Platform Motion

Motion response is also important in evaluating the performance of the hybrid system since substantial impacts can be observed. Figure 7 displays the motions of the OC4 platform, combined with WECs with flat, 90° conical, and hemispherical bottoms, for $2r/d$ = 3.0, with the motion of a single platform given as reference.

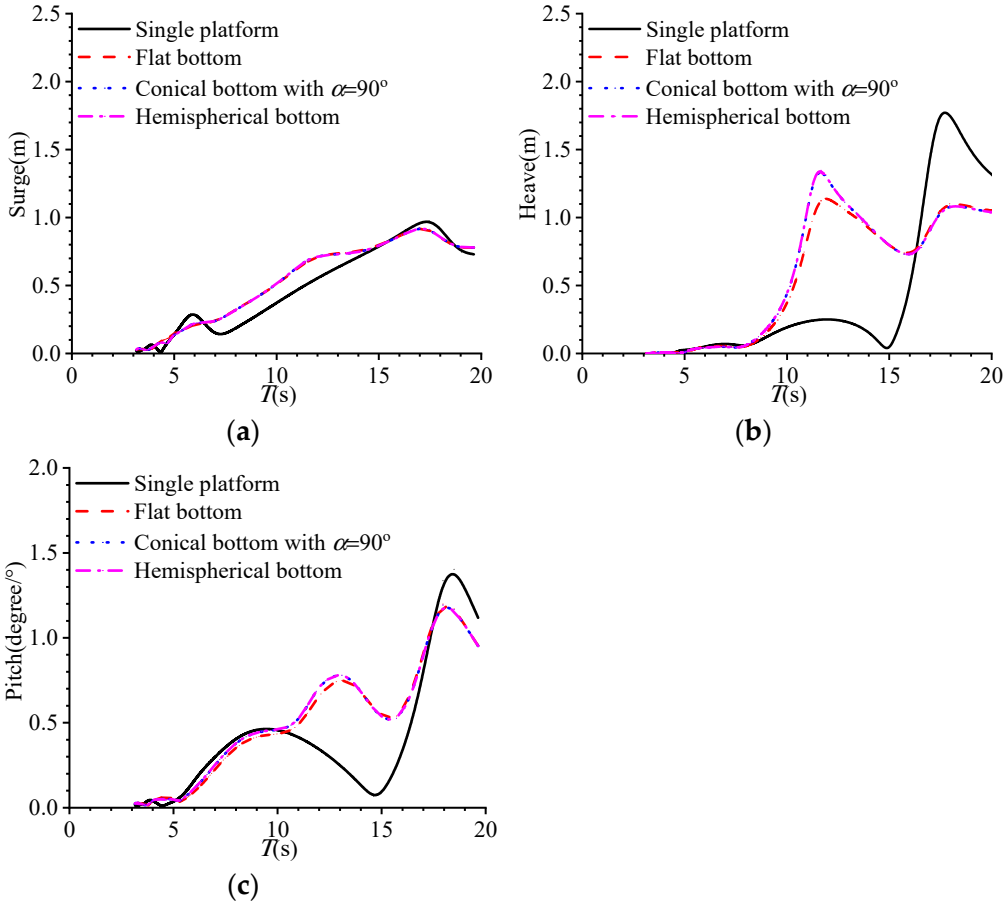

Figure 7. Motions of OC4 platform, combined with WEC with flat, 90° conical, and hemispherical bottom shapes ($2r/d$ = 3.0): (**a**) Surge; (**b**)Heave; (**c**) Pitch.

In Figure 7a, compared to the surge motion of a single platform, the platform combined with various bottom-shaped WECs manifests little increase or decrease in different wave period ranges. Bottom shapes hardly affect the surge motion of the platform.

In Figure 7b, working near the resonance period in the heave direction (i.e., T_{heave} = 17.5 s), the heave motion of the hybrid system is reduced compared to a single platform due to a viscous force caused by the addition of PTO. Whereas, in the range of 8.0 s–16.0 s, the heave motions of all three with different bottom shapes are much larger than that with

a single platform. The heave motion of the hybrid system with WECs with 90° conical and hemispherical bottoms is larger than that with conical bottoms. This variation may be consistent with the optimal PTO damping coefficient given in Figure 6a, indicating that PTO force plays a major role in the heave motion of the platform in this wave period range. In the rest waves (3.0 s–7.0 s), there is little difference in heave motion between the hybrid system with three different bottom-shaped WECs and a single platform.

In Figure 7c, variation of pitch motion is generally similar to, but not as substantial as, the behavior of heave motion in the wave period smaller than the resonance period (i.e., T_{pitch} = 20.6 s) of the platform in the pitch direction. In the range of 3.0 s–10.0 s, the hybrid system fluctuates slightly in the pitch direction. In the range of 10.0 s–17.0 s, the pitch motion of the hybrid system with WECs with 90° conical and hemispherical bottoms is slightly larger than that with conical bottoms. The pitch motions of all three with different bottom shapes are much larger than that with a single platform. In the range of 17.0 s–20.0 s, the pitch motion of the hybrid system is reduced compared to a single platform.

4.4.2. Mooring Force

Mooring horizontal force, vertical force, and pitch moment versus incident wave periods are illustrated in Figure 8, taking case $2r/d$ = 3.0, for example. Variation of mooring force (horizontal force, vertical force, and pitch moment, respectively) is similar to that of motion displacement (surge, heave, and pitch, respectively) of the platform.

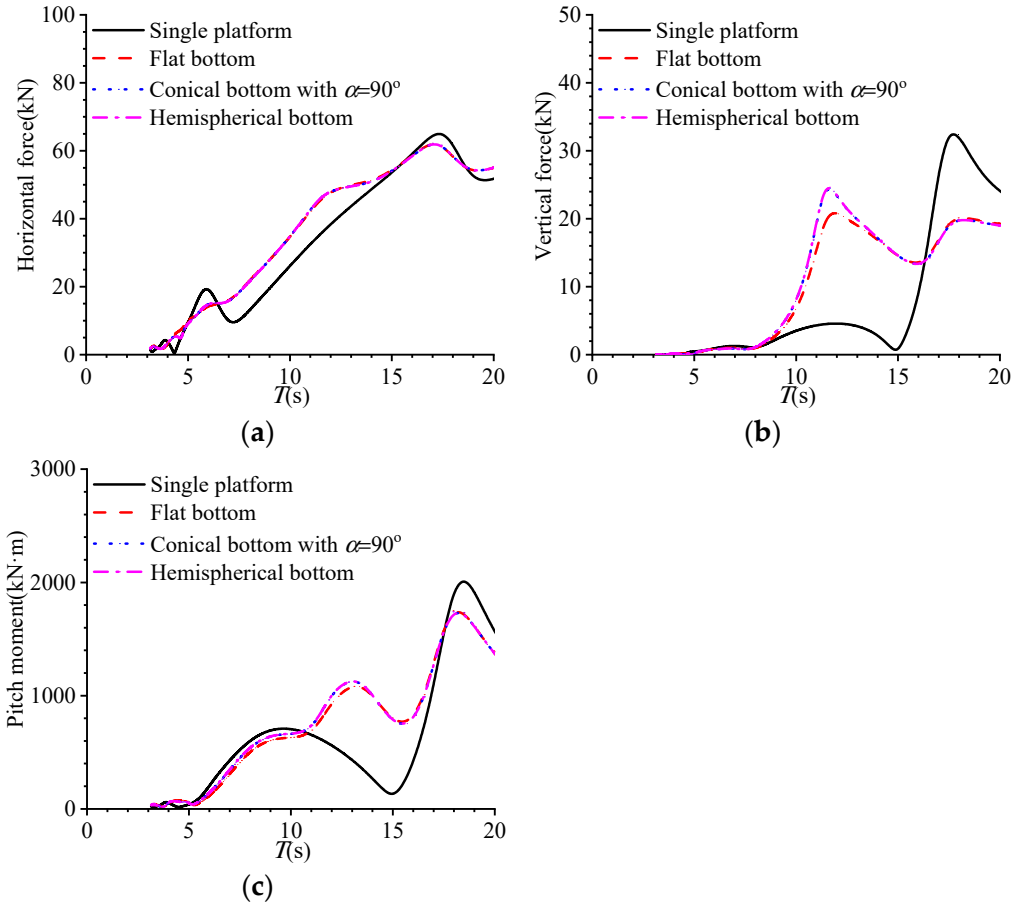

Figure 8. Variations of horizontal mooring force, vertical force, and pitch moment versus incident wave periods in the hybrid system combined with WEC with different bottom shapes ($2r/d$ = 3.0): (**a**) Horizontal force; (**b**) Vertical force; (**c**) Pitch moment.

In Figure 8a, compared to the horizontal force of a single platform, the platform combined with various bottom-shaped WECs manifests little increase or decrease in different

wave period ranges. Bottom shapes hardly affect the horizontal force of the platform. In Figure 8b, working near the resonance period in the heave direction (i.e., T_{heave} = 17.5 s) of the platform, the vertical force of the hybrid system is reduced compared to a single platform. Whereas, in the range of 8.0 s–16.0 s, the vertical forces of all three with different bottom shapes are much larger than that with a single platform. The vertical force of the hybrid system with WECs with 90° conical and hemispherical bottoms is slightly larger than that with conical bottoms. In the rest waves (3.0 s–7.0 s), there is little difference in vertical force between the hybrid system with three different bottom-shaped WECs and a single platform. In Figure 8c, in the range of 3.0 s–10.0 s, the hybrid system fluctuates slightly in pitch moment. In the range of 10.0 s–17.0 s, the pitch moment of the hybrid system with WECs with 90° conical and hemispherical bottoms is larger than that with conical bottoms. The pitch moments of all three with different bottom shapes are much larger than that with a single platform. In the range of 17.0 s–20.0 s, the pitch motion of the hybrid system is reduced compared to a single platform.

4.5. Hydrodynamic Optimization Analysis of the Distance between WECs and the Platform

Configuration of WECs is of vital importance for the performance optimization of the hybrid system. The influence of the distance L_3 of WECs protruding out the sides of the triangular frame of the platform on power performance and motion response of the hybrid system is explored, given in Figure 9. A hemispherical bottom-shaped WEC with $2r/d$ = 3.0 is chosen to be studied in an operational sea state.

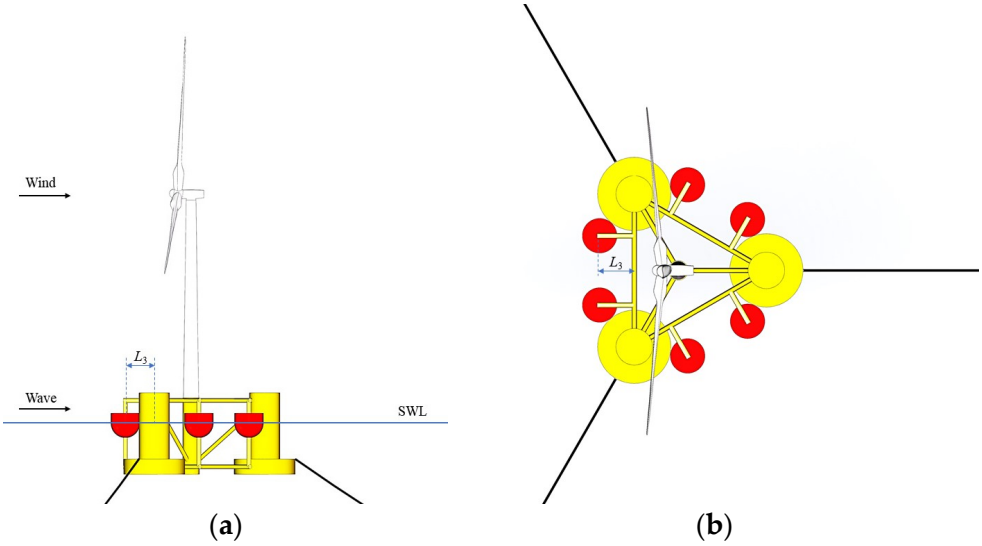

Figure 9. Diagram of the hybrid system with six heaving WECs protruding out the sides of the triangular frame of the platform: (**a**) Side view; (**b**) Top view.

4.5.1. Wave Power

Figure 10 gives the wave power of the hybrid system versus the incident wave period for various distances L_3 protruding out the sides of the triangular frame of the platform.

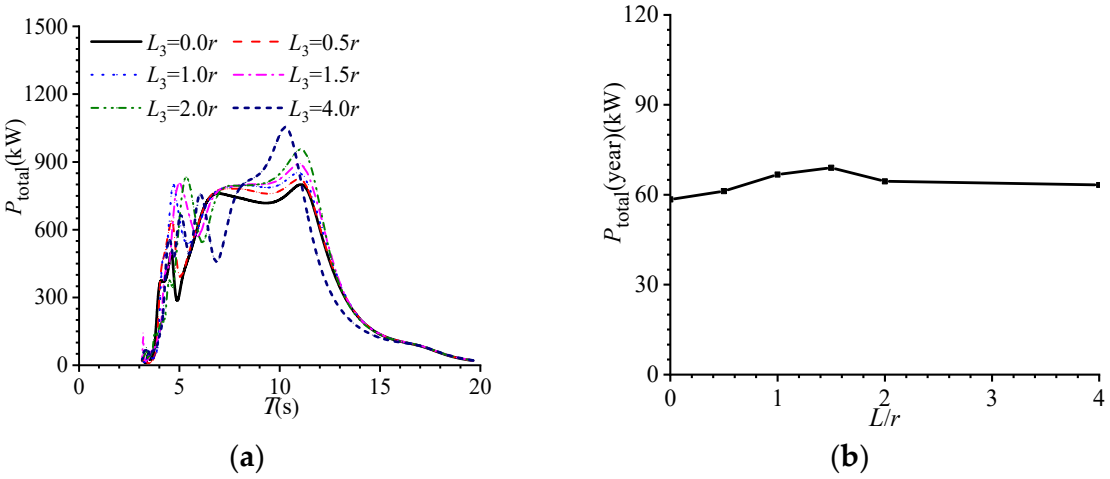

Figure 10. Variation of wave power of the hybrid system with incident wave period under various values of L_3: (**a**) Total wave power; (**b**) Annual wave power.

In Figure 10a, near the resonance period (T = 5.18 s) of the target sea, the wave period corresponding to the peak value of total wave power shifts towards a larger period. As the distance between WECs and the platform increases, the offset amplitude and the peak value of total wave power gradually become larger. Till L_3 = 4.0r, the peak value decomposes into several smaller peaks. Near T = 12.0 s, the wave period corresponding to the peak value begins to move towards a smaller period gradually. This peak value becomes larger with the increase in distance.

Figure 10b gives the annual average power generation according to Equation (8), in which the joint distributions S_{ij}, considered as the weight coefficients for different sea states, are listed in Table 3, and wave power generations per wave amplitude versus incident wave period are given in Figure 5. Hence, the annual average power generations in Figure 10b are not directed against only one sea state but are weighted based on a specific sea state. This value is 58.4 kW, 61.2 kW, 66.7 kW, 69.0 kW, 65.2 kW, and 63.4 kW, corresponding to the distance L_3 =0, 0.5r, 1.0r, 1.5r, 2.0r, and 4.0r, respectively. It can be concluded that case L_3 = 1.5r has the best annual average power generation performance of the hybrid system at the given sea state. In practical engineering applications, adjusting the distance between WEC and the sides of the triangular frame of the platform can enhance the total power performance of the hybrid system. For example, when the distance L_3 = 1.5r, wave power generation can be improved by up to 18.2%, compared to the original design method directly placed on the platform, beneficial to synergism between wave energy and wind energy.

4.5.2. Platform Motion

Figure 11 gives the surge, heave, and pitch motion of the OC4 platform for various distances L_3 with a single platform for comparison. In Figure 11a, as the distance between WEC and the sides of the platform increases, the surge motion of the platform in the range of 10.0 s–14.0 s decreases, with little difference in other ranges of wave period. In Figure 11b, except for L_3 = 4.0r, the peak value and its corresponding wave period of the heave motion of the hybrid system are seldom affected by the distance L_3. In Figure 11c, as distance L_3 increases, the peak value of pitch motion increases in the range of 8.0 s–14.0 s, and this value decreases in the range of 17.0 s–20.0 s. Meanwhile, in the range of 8.0 s–14.0 s, the wave period corresponding to the peak of pitch shifts forward to a smaller one.

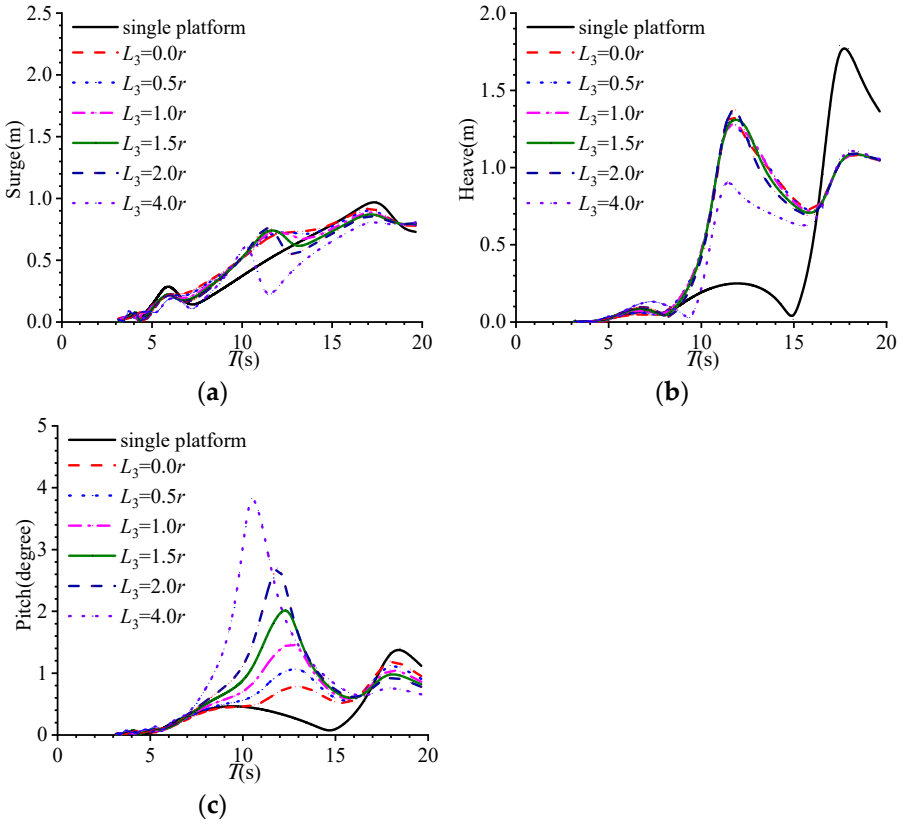

Figure 11. Variation of the platform motion with incident wave period under various values of L_3: (**a**) Surge motion; (**b**) Heave motion; (**c**) Pitch motion.

5. Conclusions

Based on a frequency-domain coupled hydrodynamic model, the shape, the PTO damping, the layout of the PAWECs combined with a semi-submersible floating wind platform are optimized, and their influences on the power performance, mooring force, and motion response of the hybrid system are explored under a wave condition measured in the Yellow Sea, China. The main conclusions are:

(1) The annual power generation of a PAWEC can be improved by 30% by using a 90° conical or hemispherical bottom instead of a flat bottom. To all of the three kinds of PAWECs using a flat, 90° conical, or hemispherical bottom, the hydrodynamic coupling changes the added mass of the PAWECs, hence their heaving natural period;

(2) Similar to the situation where the wind platform is fixed, the platform's motion does not influence the selection result of the size of the PAWECs. The larger the diameter and the diameter-to-draft ratio, the more wave power is generated;

(3) The resonant heave and pitch motion of the platform can be reduced by the power take-off damping force exerted by the PAWECs. On the other hand, the surge motion changes a little;

(4) Variation of the mooring loads (horizontal force, vertical force, and pitch moment) is similar to that of the motion responses (in the surge, heave, and pitch) of the platform;

(5) Different protruding distances L_3 similarly change the surge and heave motion responses of the platform. However, the larger the protruding distance causes, the larger the pitch motion response. There exists an optimal protruding distance where the maximum power can be achieved. In this study, this optimal power generation occurs while L_3 is 1.5 times the PAWEC radius, which is 18.2% higher than that while the PAWECs are installed on the sides of the triangular frame of the platform. This finding could be generalized to similar hybrid systems.

The frequency-domain analysis proposed for a hybrid system combining large floating platforms and WECs is fast and preferable for linear hydrodynamic analysis. However, it also has some limitations. It is applied to the simulation, assuming the motions of the structure are small amplitudes. It also cannot reflect the transient responses of the structure or the nonlinearities due to PTO systems, wave forces, mooring forces, or the compressibility of the air trapped.

The above findings can provide an approach for the hydrodynamics optimization of the layout of a wind–wave hybrid system. It illustrates a clear understanding of the influence of layout on power performance and motion response and gives a preferred configuration at an operational sea state. This study could promote the synergy of joint wave and wind energy exploitation, guiding practical engineering.

Author Contributions: Conceptualization, B.Z. and J.H.; methodology, J.H.; software, J.H.; validation, J.H. and Q.Z.; formal analysis, J.H., Q.Z. and L.W.; investigation, Q.Z.; resources, B.Z.; data curation, J.H.; writing—original draft preparation, J.H.; writing—review and editing, B.Z., F.J., L.W. and M.C.; visualization, Q.Z.; supervision, B.Z.; project administration, B.Z.; funding acquisition, B.Z. All authors have read and agreed to the published version of the manuscript.

Funding: This research was funded by Key-Area Research and Development Program of Guangdong Province (Grant No. 2020B1111010001), National Natural Science Foundation of China (Grant No. 52071096), Marine Economic Development of Guangdong, China (Grant No. GDNRC [2021]39), National Natural Science Founda-tion of China National Outstanding Youth Science Fund Project (Grant No. 52222109), Guangdong Basic and Applied Basic Research Foundation (Grant No. 2022B1515020036).

Institutional Review Board Statement: Not applicable.

Informed Consent Statement: Not applicable.

Data Availability Statement: Not applicable.

Conflicts of Interest: The authors declare no conflict of interest.

References

1. Mørk, G.; Barstow, S.; Kabuth, A.; Pontes, M.T. Assessing the global wave energy potential. In Proceedings of the ASME 2010 29th International Conference on Ocean, Offshore and Arctic Engineering, Shanghai, China, 6–11 June 2010.
2. Guo, B.Y.; Ringwood, J.V. Geometric optimisation of wave energy conversion devices: A survey. *Appl. Energy* **2021**, *297*, 117100. [CrossRef]
3. Zhou, Y.; Ning, D.Z.; Shi, W.; Johanning, L.; Liang, D.F. Hydrodynamic investigation on an OWC wave energy converter integrated into an offshore wind turbine monopile. *Coast. Eng.* **2020**, *162*, 103731. [CrossRef]
4. Perez-Collazo, C.; Pemberton, R.; Greaves, D.; Iglesias, G. Monopile-mounted wave energy converter for a hybrid wind-wave system. *Energy Convers. Manag.* **2019**, *199*, 111971. [CrossRef]
5. Zhou, Y.; Ning, D.Z.; Chen, L.F.; Iglesias, G. Nonlinear hydrodynamic modeling of an offshore stationary multi-oscillating water column platform. *Ocean Eng.* **2021**, *227*, 108919. [CrossRef]
6. Guo, B.Y.; Patton, R.; Jin, S.Y.; Gilbert, J.; Parsons, D. Nonlinear modeling and verification of a heaving point absorber for wave energy conversion. *IEEE Trans. Sustain. Energy* **2018**, *9*, 453–461. [CrossRef]
7. Jang, H.K.; Park, S.; Kim, M.H.; Kim, K.H.; Hong, K.Y. Effects of heave plates on the global performance of a multi-unit floating offshore wind turbine. *Renew. Energy* **2019**, *134*, 526–537. [CrossRef]
8. Cheng, Y.; Du, W.M.; Dai, S.S.; Ji, C.Y.; Collu, M.; Cocard, M.; Cui, L.; Yuan, Z.M. Hydrodynamic characteristics of a hybrid oscillating water column-oscillating buoy wave energy converter integrated into a π-type floating breakwater. *Renew. Sustain. Energy Rev.* **2022**, *161*, 112299. [CrossRef]
9. Ning, D.Z.; Zhao, X.L.; Zhao, M.; Hann, M.; Kang, H.G. Analytical investigation of hydrodynamic performance of a dual pontoon WEC-type breakwater. *Appl. Ocean Res.* **2017**, *65*, 102–111. [CrossRef]
10. Zhou, B.Z.; Zheng, Z.; Zhang, Q.; Jin, P.; Wang, L.; Ning, D.Z. Wave attenuation and amplification by an abreast pair of floating parabolic breakwaters. *Energy* **2023**, *271*, 127077. [CrossRef]
11. Cheng, Z.S.; Wang, K.; Gao, Z.; Moan, T. A comparative study on dynamic responses of spar-type floating horizontal and vertical axis wind turbines. *Wind Energy* **2017**, *20*, 305–323. [CrossRef]
12. Clark, C.E.; Miller, A.; DuPont, B. An analytical cost model for co-located floating wind-wave energy arrays. *Renew. Energy* **2019**, *132*, 885–897. [CrossRef]
13. Zhou, B.Z.; Ding, K.L.X.; Wang, J.H.; Wang, L.; Jin, P.; Tang, T.N. Experimental study on the interactions between wave groups in double-wave-group focusing. *Phys. Fluids* **2023**, *35*, 037118. [CrossRef]

14. Oliveira-Pinto, S.; Rosa-Santos, P.; Taveira-Pinto, F. Assessment of the potential of combining wave and solar energy resources to power supply worldwide offshore oil and gas platforms. *Energy Convers. Manag.* **2020**, *223*, 113299. [CrossRef]
15. Pérez-Collazo, C.; Greaves, D.; Iglesias, G. A review of combined wave and offshore wind energy. *Renew. Sustain. Energy Rev.* **2015**, *42*, 141–153. [CrossRef]
16. Cheng, Y.; Dai, S.Q.; Dai, S.S.; Ji, C.Y.; Collu, M.; Yuan, Z.M.; Incecik, A. Energy conversion and hydrodynamic analysis of multi-degree-of-freedom wave energy converters integrated into a semi-submersible platform. *Energy Convers. Manag.* **2022**, *252*, 115075. [CrossRef]
17. Marina Platform. European Union Seventh Framework Programme (EU FP7) Marine Renewable Integrated Application Platform MARINA Platform. Available online: https://cordis.europa.eu/project/rcn/93425_en.html (accessed on 9 May 2023).
18. M'zoughi, F.; Aboutalebi, P.; Garrido, I.; Garrido, A.J.; De La Sen, M. Complementary airflow control of oscillating water columns for floating offshore wind turbine stabilization. *Mathematics* **2021**, *9*, 1364. [CrossRef]
19. Aboutalebi, P.; M'zoughi, F.; Garrido, I.; Garrido, A.J. Performance analysis on the use of oscillating water Column in Barge-based floating offshore wind turbines. *Mathematics* **2021**, *9*, 475. [CrossRef]
20. Michailides, C.; Gao, Z.; Moan, T. Experimental study of the functionality of a semisubmersible wind turbine combined with flap-type Wave Energy Converters. *Renew. Energy* **2016**, *93*, 675–690. [CrossRef]
21. Michailides, C.; Gao, Z.; Moan, T. Experimental and numerical study of the response of the offshore combined wind/wave energy concept SFC in extreme environmental conditions. *Mar. Struct.* **2016**, *50*, 35–54. [CrossRef]
22. Muliawan, M.J.; Karimirad, M.; Moan, T. Dynamic response and power performance of a combined Spar-type floating wind turbine and coaxial floating wave energy converter. *Renew. Energy* **2013**, *50*, 47–57. [CrossRef]
23. Ghafari, H.R.; Ghassemi, H.; He, G.H. Numerical study of the Wavestar wave energy converter with multi-point-absorber around DeepCwind semisubmersible floating platform. *Ocean Eng.* **2021**, *232*, 109177. [CrossRef]
24. Karimirad, M.; Michailides, C. Effects of misaligned wave and wind action on the response of the combined concept windWEC. In Proceedings of the ASME 2018 37th International Conference on Ocean, Offshore and Arctic Engineering, Madrid, Spain, 17–22 June 2018.
25. Cheng, Z.S.; Wen, T.R.; Ong, M.C.; Wang, K. Power performance and dynamic responses of a combined floating vertical axis wind turbine and wave energy converter concept. *Energy* **2019**, *171*, 190–204. [CrossRef]
26. Ren, N.X.; Ma, Z.; Shan, B.; Ning, D.Z.; Ou, J.P. Experimental and numerical study of dynamic responses of a new combined TLP type floating wind turbine and a wave energy converter under operational conditions. *Renew. Energy* **2020**, *151*, 966–974. [CrossRef]
27. Wang, Y.P.; Zhang, L.X.; Michailides, C.; Wan, L.; Shi, W. Hydrodynamic response of a combined wind–wave marine energy structure. *J. Mar. Sci. Eng.* **2020**, *8*, 253. [CrossRef]
28. Wang, Y.P.; Shi, W.; Michailides, C.; Wan, L.; Kim, H.; Li, X. WEC shape effect on the motion response and power performance of a combined wind-wave energy converter. *Ocean Eng.* **2022**, *250*, 111038. [CrossRef]
29. Hu, J.J.; Zhou, B.Z.; Vogel, C.; Liu, P.; Willden, R.; Sun, K.; Zang, J.; Geng, J.; Jin, P.; Cui, L.; et al. Optimal design and performance analysis of a hybrid system combing a floating wind platform and wave energy converters. *Appl. Energy* **2020**, *269*, 114998. [CrossRef]
30. Zhou, B.Z.; Hu, J.J.; Sun, K.; Liu, Y.Y.; Collu, M. Motion response and energy conversion performance of a heaving point absorber wave energy converter. *Front. Energy Res.* **2020**, *8*, 553295. [CrossRef]
31. Zhou, B.Z.; Hu, J.J.; Jin, P.; Sun, K.; Li, Y.Y.; Ning, D.Z. Power performance and motion response of a floating wind platform and multiple heaving wave energy converters hybrid system. *Energy* **2023**, *265*, 126314. [CrossRef]
32. Robertson, A.; Jonkman, J.; Masciola, M.; Song, H. *Definition of the Semisubmersible Floating System for Phase II of OC4*; Technical Report NREL/TP 5000-60601; National Renewable Energy Laboratory: Golden, CO, USA, 2014.
33. Masciola, M.; Jonkman, J.; Robertson, A. Extending the capabilities of the mooring analysis program: A survey of dynamic mooring line theories for integration into FAST. In Proceedings of the 33rd International Conference on Offshore Mechanics and Arctic Engineering, American Society of Mechanical Engineers, San Francisco, CA, USA, 8–13 June 2014.
34. Ruehl, K.; Michelen, C.; Kanner, S. Preliminary verification and validation of WEC-Sim, An open-source wave energy conversion design tool. In Proceedings of the 33rd International Conference on Offshore Mechanics and Arctic Engineering, American Society of Mechanical Engineers, San Francisco, CA, USA, 8–13 June 2014.
35. Zhang, H.M.; Zhou, B.Z.; Vogel, C.; Willden, R.; Zang, J.; Geng, J. Hydrodynamic performance of a dual-floater hybrid system combining a floating breakwater and an oscillating-buoy type wave energy converter. *Appl. Energy* **2020**, *259*, 114212. [CrossRef]
36. Zhang, H.M.; Zhou, B.Z.; Vogel, C.; Willden, R.; Zang, J.; Zhang, L. Hydrodynamic performance of a floating breakwater as an oscillating-buoy type wave energy converter. *Appl. Energy* **2020**, *257*, 113996. [CrossRef]